Mon. Not. R. Astron. Soc. **000**, 000–000 (0000) Printed 20 May 2005 (MN LaTeX style file v2.2)

Morphological Studies of the SWIRE Galaxy Population in the UGC 10214 HST/ACS field

E. Hatziminaoglou[1], P. Cassata[2], G. Rodighiero[2], I. Pérez-Fournon[1],
A. Franceschini[2], A. Hernán-Caballero[1], F.M. Montenegro-Montes[1]
A. Afonso-Luis[1], T. Jarrett[3], G. Stacey[4], C. Lonsdale[5], F. Fang[4], S. Oliver[6],
Rowan-Robinson[7], D. Shupe[3], H.E. Smith[5], J. Surace[3], C.K. Xu[3]
[1] *Institute de Astrofisica de Canarias, C/ Via Lactea s/n, E-38200 La Laguna, Spain*
[2] *Dipartimento di Astronomia, Universita di Padova, Vicolo Osservatorio 5, 35122 Padua, Italy*
[3] *Infrared Processing and Analysis Center, California Institute of Technology, Pasadena, CA 91125, USA*
[4] *Cornell University, Astronomy Department, Ithaca, NY 14853, USA*
[5] *Center for Astrophysics and Space Sciences, University of California, San Diego, La Jolla, CA 92093-0424, USA*
[6] *Astronomy Centre, Department of Physics and Astronomy, University of Sussex, Falmer, Brighton BN1 9QJ, UK*
[7] *Astrophysics Group, Blackett Laboratory, Imperial College London, London SW7 2BW, UK*

20 May 2005

ABSTRACT

We present results of a morphological analysis of a small subset of the Spitzer Wide-area InfraRed Extragalactic survey (SWIRE) galaxy population. Our reference sample is flux-limited at 3.6 and 4.5 μm and includes 156 galaxies with flux densities $S \geqslant 10$ μJy. Our analysis is based on public ACS data taken inside the SWIRE N1 field, which are the deepest optical high-resolution imaging available within the SWIRE fields as of today. Among the various galaxy morphologies, we disentangle two main classes, spheroids (or bulge-dominated galaxies) and disk-dominated ones, for which we estimate the number counts as a function of flux. We find that the observed counts of the spheroidal population agree with the expectations of a hierarchical model while a monolithic scenario predicts much steeper counts. Both scenaria, however, under-predict the number of late-type galaxies. These observations show that the large majority of the Spitzer galaxy population (close to 80 per cent), even at these moderately faint fluxes, is dominated by spiral and irregular galaxies or mergers.

Key words: galaxies: evolution – galaxies: elliptical and lenticular, cD – galaxies: spiral – galaxies: irregular – infrared: general – infrared: galaxies

1 INTRODUCTION

A key question on galaxy formation and evolution, in particular about the early-type sub-population which includes the most massive galaxies at any redshifts, is when and on which timescales their stellar content has been formed and assembled. Two schematic models are often confronted with the observations, the monolithic collapse model (Eggen et al. 1962; Larson 1975; Chiosi & Carraro 2002) and the hierarchical assembly scenario (e.g. White & Rees 1978; White & Frenk 1991; Somerville & Primack 1999; Cole et al. 2000). In the monolithic collapse, a burst of star formation happened at very high redshifts ($z_{form} \geqslant 3$) and was followed by passive evolution of the stellar populations, whereas in the hierarchical assembly scenario the timescales for more massive galaxies are longer, resulting in somewhat younger mean ages. According to the latter interpretation, ellipticals are formed by mergers and/or accretion of smaller galaxies over timescales comparable to the Hubble time.

Fundamental observational constraints on the star formation history and the formation pattern are provided by the broad-band colours, line strength indexes and stellar chemical abundances. When referred to massive ellipticals, these data suggest that the bulk of stars might have been formed in a remote past. However, some secondary activity of star formation in the recent past is also evident: nearby ellipticals show a large variety of morphological and kinematic peculiarities (e.g. Longhetti et al. 2000) and a substantial spread of stellar ages, particularly for the field population (Thomas et al. 2005). Strong evolution in the population of early-type galaxies has been reported by Kauffmann et al. (1996) and Kauffmann & Charlot (1998) which has been considered to support the hierarchical galaxy formation models.

The current results about the number counts and redshift distributions of the evolved galaxies at high redshift are still rather inconclusive, and theoretical models about their formation and evolution are correspondingly uncertain (see Somerville et al. 2004 for a brief review).

Near-IR surveys are best suited for the study of faint high-redshift galaxy populations, for various reasons: the observed fluxes are minimally influenced by K-corrections and only weakly affected by dust extinction, and at the same time good indicators of the stellar mass content of galaxies (Dickinson et al. 2003). Mid-IR observations, on their side, are strongly informative about phases of active star formation in galaxies (Franceschini et al. 2001; Rowan-Robinson 2001; Xu et al. 2003 and many others). After the ISO exploratory observations, the Spitzer Space Observatory mission has started to map systematically the high-redshift universe at such long wavelengths.

The main aim of the Spitzer Wide-area InfraRed Extragalactic survey (SWIRE) is the study of the evolution of both actively star-forming and passively-evolving galaxies, by exploiting a huge sample of some 2 million galaxies that are detected within the ~ 50 deg^2 of the survey.

Good quality optical data are essential for the identification and characterization of Spitzer sources. However, typical images obtainable from ground are not adequate for accurate morphological analyses and source classification. In this paper we exploit very deep multiband public images taken with the Advanced Camera for Surveys (hereafter ACS; Ford et al. 1998) in a small portion of the SWIRE N1 field, in order to study the morphological properties of the mid-IR (MIR) and near-IR emitting galaxies.

Section 2 of the paper describes the optical (HST/ACS) and IR (Spitzer) data used in our analysis. Section 3.1 gives a brief description of the tools used for the morphological analysis and classification as well as a comparison of their results. Section 4 describes a comparison of our modelistic galaxy number counts with our observational data. Finally, sections 4.3 and 5 summarise our results and conclusions.

2 THE DATA

SWIRE N1 was the first field to be observed by Spitzer for the SWIRE Legacy program. The MIR data used here were obtained in February 2004 and the SWIRE catalogues we use throughout this work were processed by the SWIRE team. Source extraction was performed using *SExtractor* (Bertin & Arnouts 1996) with local background mesh subtraction. Kron and 2.9" aperture fluxes were used here, for extended and point-like sources, respectively. The Kron fluxes were extracted within a minimum radius of 2" using a Kron factor of 2.5. These fluxes were the *default* fluxes in the first SWIRE data release. The astrometric accuracy is better than 1". More details about the entire data set can be found in Lonsdale et al. 2004, Surace et al. 2005 and Shupe et al. 2005.

The optical data were obtained with the ACS on the Hubble Space Telescope. The field is centred on UGC 10214 (also known as VV 29 and Arp 188, the *Tadpole* galaxy), a bright spiral at $z = 0.032$ with a huge tidal tail. The optical

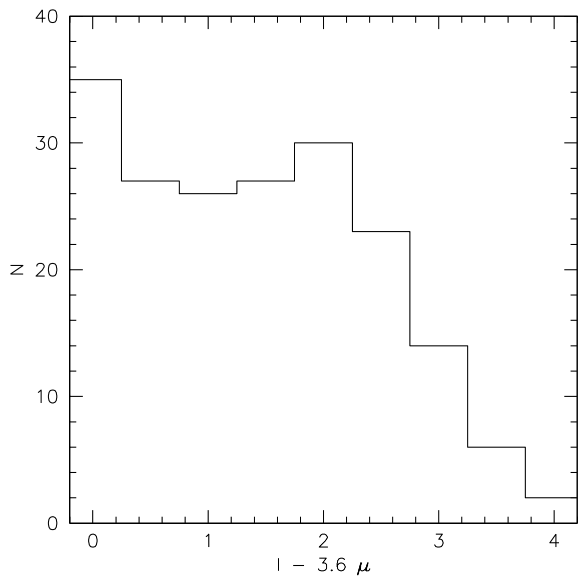

Figure 2. (I-3.6µm)$_{AB}$ colour histogram for the matched SWIRE-ACS sources.

catalogue contains some 5700 objects with 10 σ detection limits for point sources of of 27.8, 27.6 and 27.2 AB magnitudes in the $g_{\rm F475W}$, $V_{\rm F606W}$ and $I_{\rm F814W}$ bands respectively. For details on the data reduction and catalogue production see Benitez et al. 2004. This field lies close to the centre of the SWIRE N1 field, providing an unprecedented opportunity of combining very deep optical data with high quality MIR and near-IR data in wavelength ranges so far poorly explored.

Within the ~14 sq. arcmin ACS field, we use an area of ~10 sq. arcmin well outside the region occupied by the UGC 10214 galaxy. The matching between the SWIRE and ACS sources was done using the TMATCH task of *IRAF*, with an 1" match radius. The sources were then visualised one by one and a flag was assigned to each one of them, stating their status with respect to close counterparts. Out of the 177 matched objects, 175 and 130 are detected in 3.6 and 4.5 µm , respectively (with two having only 4.5 µm detections) and 18 (i.e. ~ 10%) have at least two extracted ACS counterparts within an 1" radius. For a detailed discussion of the optical/MIR bandmerged catalogues and the spectral energy distribution (SED) of the matched objects we defer to Pérez-Fournon et al. (in preparation) and Hernán-Caballero et al. (in preparation).

The I-band counts for the entire ACS field and for the sources with a SWIRE counterpart are shown in Fig. 1 in solid and in dashed lines, respectively. Down to a magnitude of I∼ 22.5 almost all ACS sources have a MIR counterpart, while the numbers starts dropping below I∼ 23.5, reflecting the shallowness of the SWIRE data. The completeness of the 3.6 µm counts drops quickly below 10 µJy, value corresponding to an AB limiting magnitude of 21.4 or I∼ 23.5 for a typical I-3.6µm colour of 2 (see Fig. 2 for the colour distribution of the 177 matched sources).

Note that the probability of chance associations within 1" of radius is of less than 2% up to an I-band magnitude of 24.0 and up to 5% at an I-band magnitude of 25. Tak-

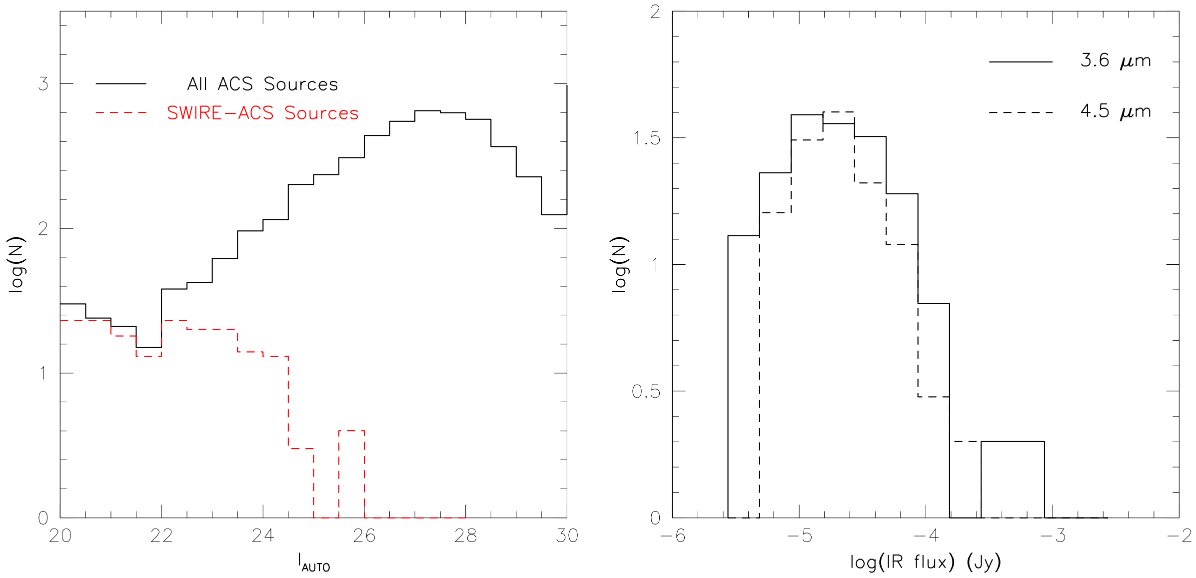

Figure 1. Left panel: I-band number counts for all ACS sources (solid line) and for the SWIRE-ACS identifications (dashed line) in the ~ 10 sq. arcmin field covered by the ACS observations, after the area around UGC 10214 has been removed. Right panel: 3.6 μm (solid line) and 4.5 μm (dashed line) distribution of the SWIRE-ACS sources.

ing into account the I-band magnitude distribution of the SWIRE sources (Fig. 1), one expects less than 5 out of the 177 sources to be wrongly matched.

3 MORPHOLOGICAL CLASSIFICATION

3.1 Tools for the morphological analysis

A number of parametric and non-parametric methods are suggested in the literature for quantitative assessment of the morphological properties of intermediate and high redshift galaxies. Among the parametric approaches, an often used representation of the galaxy morphological types is the Sérsic index, n, which appears in the surface brightness profile law $I_r = I_b(0)e^{-b_n(r/r_m)^{1/n}}$, where $I_b(0)$ is the bulge central intensity, r_m is the bulge semi-major effective radius and n the Sérsic shape parameter (Sérsic 1968). The quantity b_n is a function of n, and is chosen so that r_m encloses half of the total luminosity. The Sérsic profile includes the classical de Vaucouleurs profile when n is equal to 4.

Alternatively, non-parametric approaches have been proposed, with the most common one using the combination of the light Concentration (C), Asymmetry (A) and clumpinesS (S), or CAS, parameters. Concentration (Abraham et al. 1996) roughly correlates with the Sérsic index, while asymmetry (Conselice et al. 2000) compares the image of a source with its rotated (usually by 180°) counterpart, enabling the distinction between normal and irregular galaxies or merging systems. The clumpiness, (Conselice 2003), measures the uniformity of the light distribution in a galaxy. Abraham et al. (1996) and later on (Conselice et al. 2000) showed that bulge-dominated, disk-dominated and merging systems occupy different but often overlapping regions in the Asymmetry - Concentration space. Conselice (2003) finally demonstrated that all galaxy types can be clearly identified by their position in the *CAS* three-dimensional space.

Our morphological analysis has been performed in three independent steps: i) visual inspection, in order to attribute each object to a given morphological class based on features like the presence of spiral arms and/or bars, signs of interaction, multiple nuclei etc.; ii) a non-parametric analysis of the galaxy light distribution using the CAS parameters (see Conselice et al. 2003 for a detailed description and Cassata et al. 2005 for their exact definition as used here); iii) a detailed analysis of the surface brightness profiles using the packages GALFIT (Peng et al. 2000) and GASPHOT (Pignatelli et al. 2005).

3.2 Results of the morphological analysis

In the 10.56 sq. arcmin region of the ACS field uncontaminated by UGC 10214, there are 177 objects with a SWIRE counterpart. As a first step, a visual inspection of these sources was carried out on the I-band image by three of the authors, independently. The individual results were then compared and finally combined after the very few dubious cases were discussed (the excellent quality of the ACS data allows for very little doubt about the morphological characteristics of the objects at these relatively bright magnitudes). The visual analysis identifies four main groups of objects: *spheroids* (consisting of ellipticals and S0 galaxies), *spirals*, *irregular* galaxies and *pairs* and found four objects too faint to be classified; 21 were stars (stars were double-checked adopting the criterion of Benitez et al. 2004 for stellar classification, i.e. a SExtractor CLASS_STAR $\geqslant$ 0.94); 37 spheroids; 69 spiral galaxies; 24 irregulars and 22 merger or interacting systems or sources with multiple components (all characterised as *pairs*). Fig. 3 shows examples of each of the categories along with their CAS parameters, discussed hereafter.

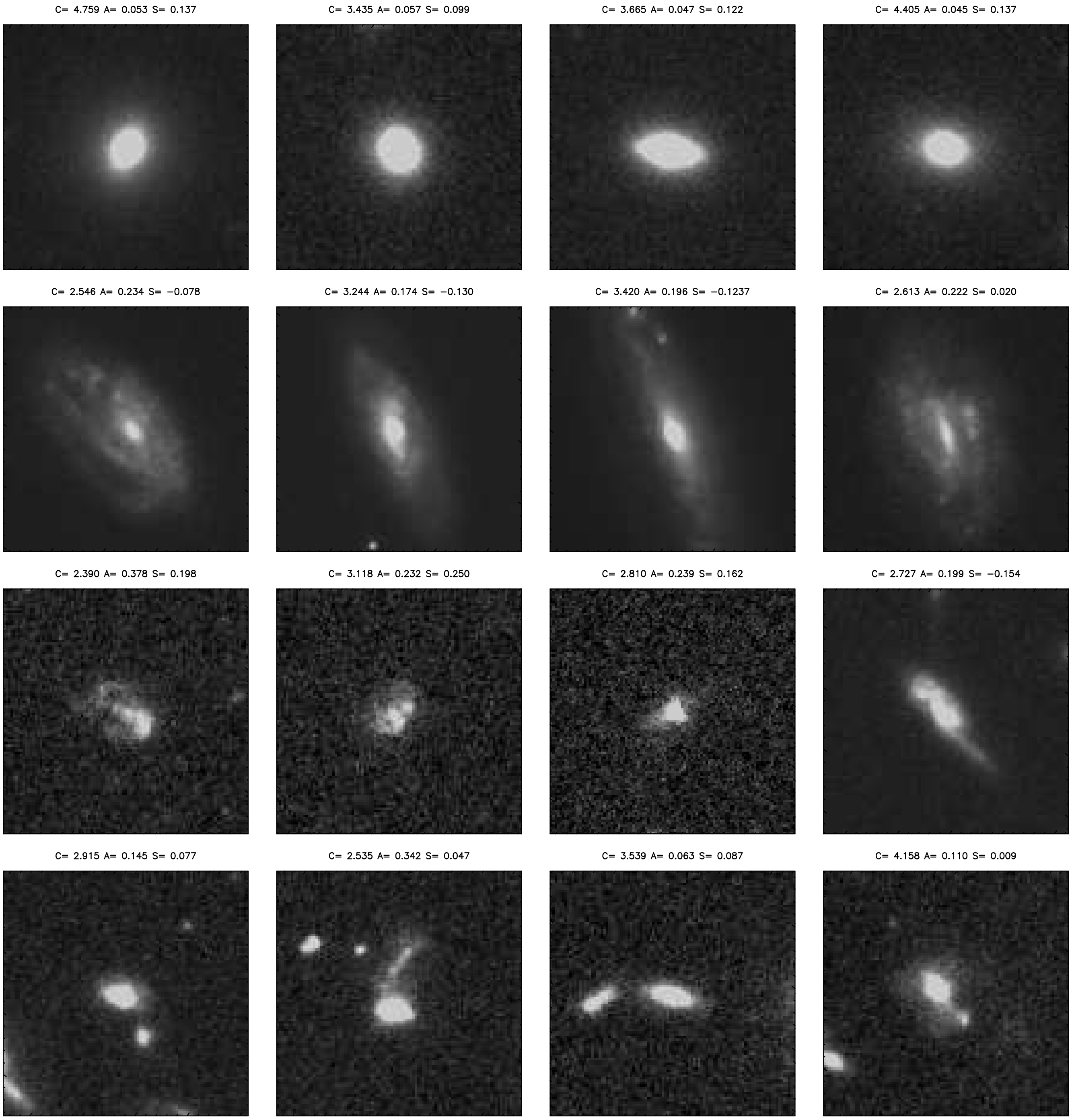

Figure 3. Examples of objects visually classified as ellipticals, spirals, irregulars and pairs (from upper to lower row) and their CAS parameters. The size of the cutouts is of 5 × 5 arcsec.

For nearly a quarter of the 156 galaxies (the 21 stars are from now on excluded), CAS parameters were not computed. Before computing CAS, pixels below 2× RMS are filtered out (corresponding to 25 mag/arcsec^2). For objects with no pixels above this level the A and S are not computed. The computation of C makes use of the SExtractor-derived growth curve of each object and no filter is applied on the image. Furthermore, for objects with complex structure (visually classified as pairs or irregular galaxies), their multiple components or uncommon shape render the CAS analysis difficult. For the rest of the sources, however, this approach gave results largely in agreement with the visual inspection. Spheroids tend to have lower A and higher C than spirals, irregulars or pairs and tend to concentrate around $S \sim 0.1$. In fact, 35 of the 37 visually classified spheroids lie in or at the very borders of the region shown in Fig. 4, defined by:

$$A < 0.2 \,\&\, C > 2.7 \qquad (1)$$

$$C > 2.7 \,\&\, 0.0 \leqslant S < 0.3 \qquad (2)$$

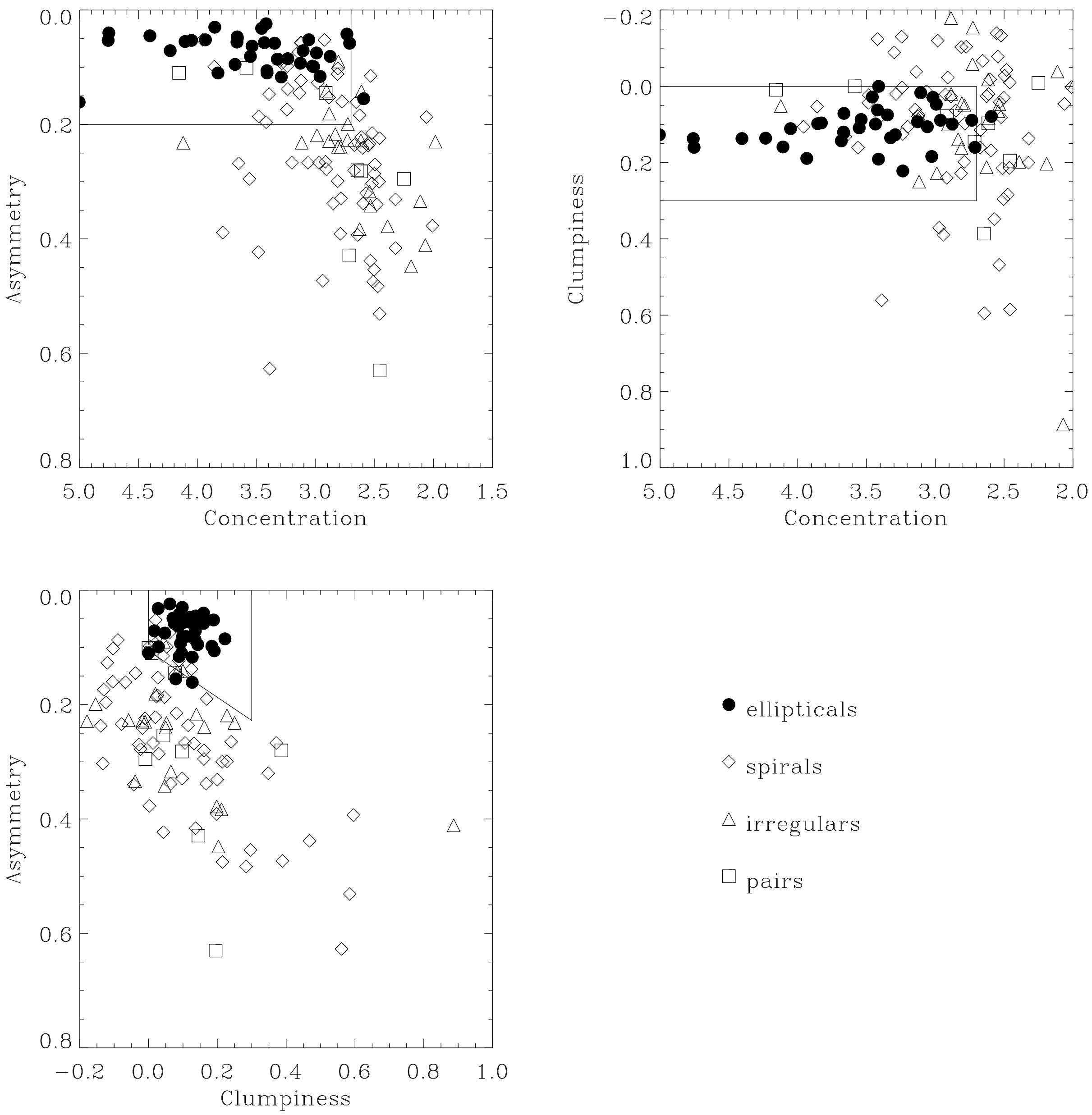

Figure 4. Asymmetry, Concentration and Clumpiness for the SWIRE-ACS sources and comparison with the classification obtained by visual inspection.

$$0.0 \leqslant S < 0.3 \,\&\, 3A - S < 0.3 \tag{3}$$

One of the remaining two objects lies outside but close to the delineated region (seen in all three diagrams of Fig. 4) while for the last one, shown in Fig. 5, the *CAS* code didn't converge, possibly because of its asymmetric shape or the presence of the faint elongated structure close-by.

An additional set of 10 objects fall within this same region. Those objects are spirals but at least seven of them have prominent bulge components, as seen on the cutouts illustrated in Fig. 6. Not that for some of them it is difficult to see the spiral arms or disk components on the cutouts due to the chosen contrast but they are clear enough on the actual image for the objects to be classified as spirals. We therefore deduce that more than 90% of the objects in the designated area of the CAS parameter space are ellipticals or bulge-dominated spirals.

This analysis sets the lower and upper limits of the number of spheroids in 37 (visually classified) and 45 (included in the region delineated by Eqs. 1-3), respectively, within the ~ 10 sq. arcmin of effective area of the UGC 10214 ACS field.

The results of the parametric methods are more difficult to interpret. For low asymmetry objects the results of GALFIT and GASPHOT are in reasonable agreement with each other (Fig. 7) but discrepancies arise for the objects with with $A > 0.25$. This is somewhat expected as the less

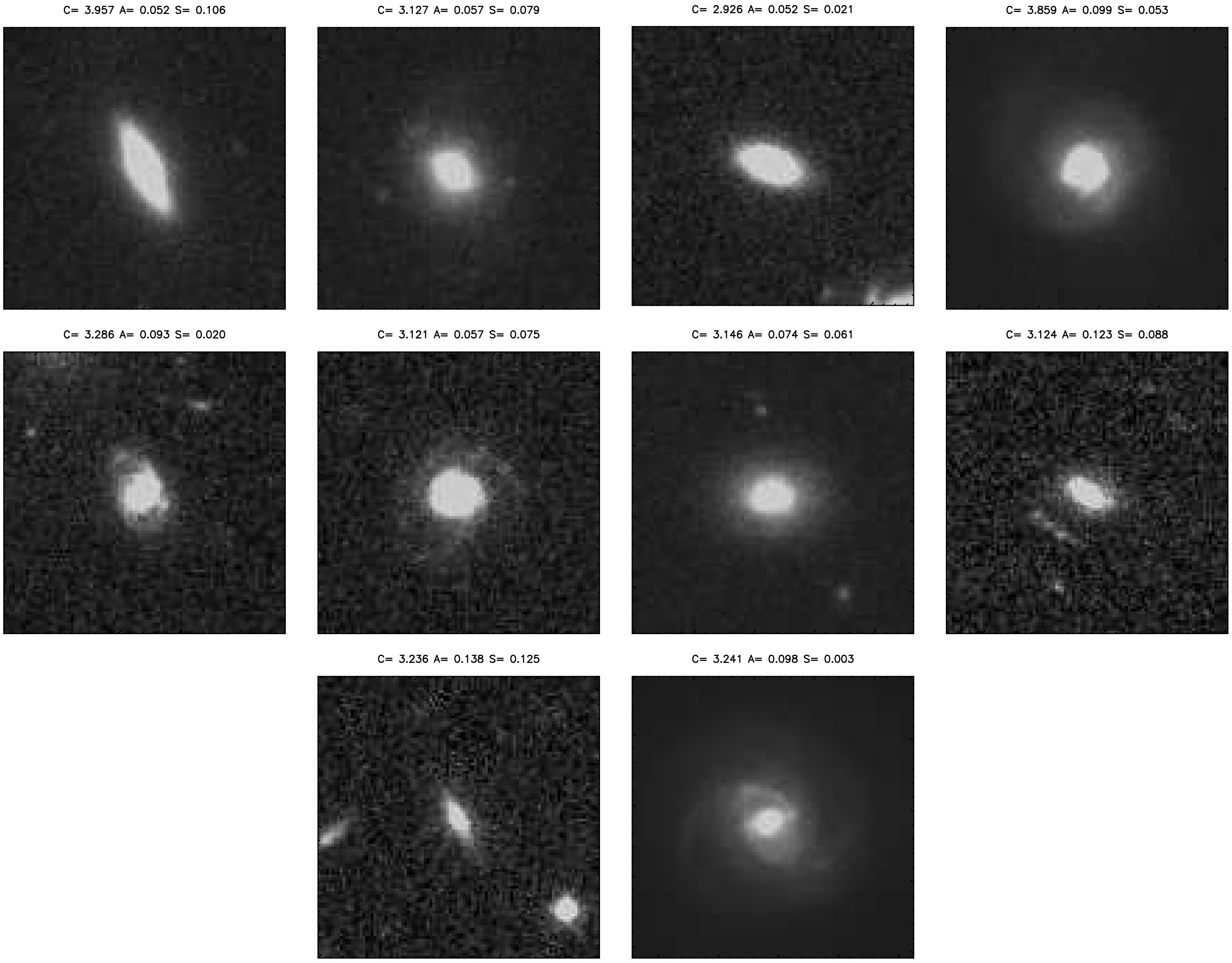

Figure 6. The ten objects visually classified as spirals that lie in the *CAS* spheroid region.

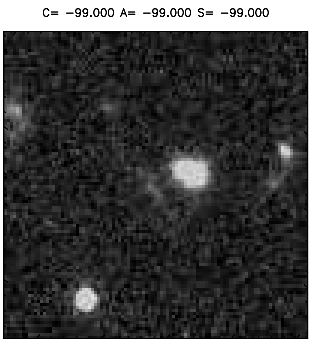

Figure 5. A visually classified elliptical for which the *CAS* code failed to converge.

symmetric galaxies can not be easily reproduced by parametric models that are intrinsically symmetric (see Cassata et al. 2005 and Pignatelli et al. 2005 for further details on the comparison between GASPHOT and GALFIT on real and simulated galaxies, respectively). Parametric and non parametric approaches also agree up to a point, with the Sérsic index, n, correlating with C in the majority of the cases (Fig. 8). Some 15 sources, however, present large deviations. For these objects the errors on the estimated values of n, R_e and M_{tot} are very large due to their nature: they are all pairs, sources with multiple components or (just one case) objects with very small isophotal area.

The distribution of Séric index, n, given by GALFIT peaks at value around 1 for late-type and around 2 for early-type galaxies. The 33 per cent of galaxies visually classified early types have and n lower than 2, and about the same percentage of late-type galaxies have n greater than 2. Among the early type galaxies with a low value of the Sérsic index, a large fraction are S0 galaxies while a certain number have a too small isophotal area to get reliable fits of the surface brightness distribution. Finally, the largest part of late-type galaxies having large Sérsic indexes is mostly composed by bulge dominated systems or again objects occupying too small isophotal areas.

The entire morphological analysis may be subject to an, unaccounted for, morphological K-correction. Morphological classification performed at a given band suffers from this effect as galaxies of higher redshifts are actually observed at bluer restframe wavelengths (Windhorst et al. 2002; Pa-

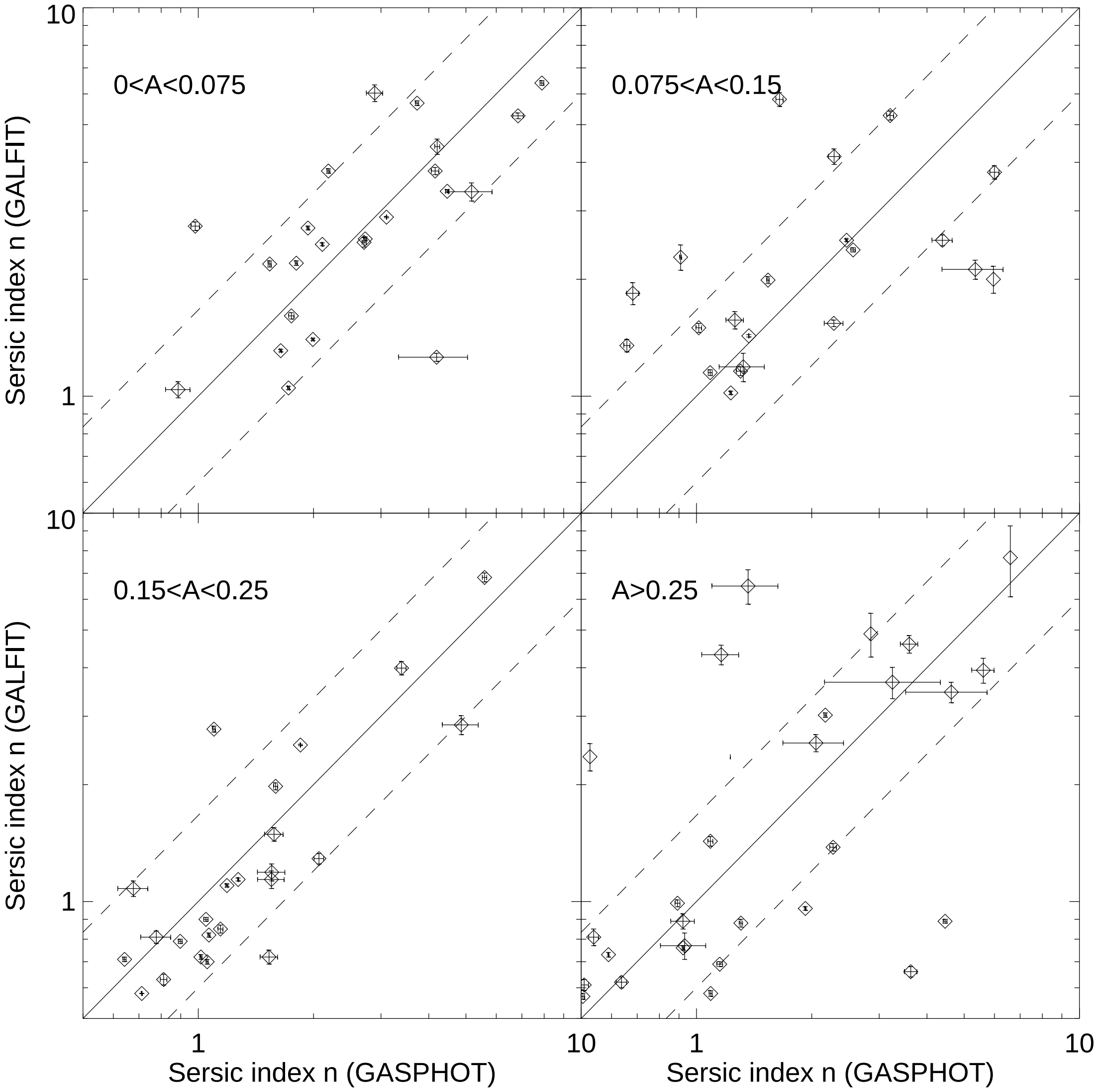

Figure 7. Sérsic index, n, computed by GALFIT versus n computed by GASPHOT for the SWIRE-ACS sources, in bins of Asymmetry. The two tools provide comparable results for low asymmetry objects. The dashed lines mark the region where $\Delta n/\bar{n} \leqslant 0.5$.

povich et al. 2003; Cassata et al. 2005). Windhorst et al. (2002) found that the morphology of galaxies changes when moving from the optical to the UV passbands. However, our analysis should not be much affected by this effect as we do not expect a large number of high redshift galaxies, due both to the relatively bright fluxes and to the very small size of the field. This, in fact, somewhat insures that we study galaxies with restframe between B- and I- bands. In particular, the number of high-redshift spheroids, population we are mostly interested in, must be particularly low. Rowan-Robinson et al. (2005), based on photometric redshift estimations and model predictions, showed that no more than 25% of the 3.6 μm galaxy sample down to a limit of 10 μJy have redshifts larger than ∼1, the largest fraction of which are late-type objects. CAS analysis may also suffer from the effects of the morphological K-correction (see i.e. Conselice et al. 2000; Lotz et al. 2004), as in general, moving toward shorter wavelengths results in larger values of A and S and smaller C. However, since we ignore the real redshifts of our objects and decided not to rely upon the photometric redshifts provided by Benitez et al. (2004) – calculated based on three optical passbands only – in order to avoid introducing further uncertainties, we chose not to apply any kind of correction, as this would probably only increase the scatter of the points in Fig. 4.

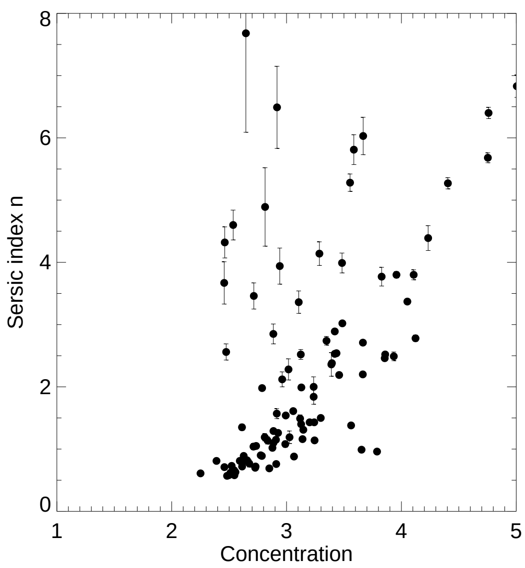

Figure 8. Sérsic index, n, computed by GALFIT versus Concentration, C. n scales with C in the majority of cases. The objects with the largest scatter are also those with the largest error bars and, in the majority of cases, have been visually classified as pairs (including systems with various components).

4 GALAXY NUMBER COUNTS

4.1 Observed number counts

The IRAC1 and IRAC2 channel (3.6 and 4.5 µm) observed cumulative galaxy counts, normalised to one square degree, are reported in Fig. 9. The various morphological classes are these derived from the visual inspection. We confine our analysis to fluxes brighter than 10 µJy in the two bands, and assume that the sample is complete here (Surace et al. 2005).

It is interesting to note here that the IRAC channels 1 & 2 are optimally suited for the identification and analysis of spheroidal galaxy populations. We have performed an automated analysis of the I-band images over entire ACS field using the CAS parameter set and found that only $\sim 7\%$ of the galaxies to the survey limit I=27.2 lie in the area defined by Eqs. 1 – 3, and are therefore classifiable as spheroids. The same analysis performed on the counterparts of the SWIRE IRAC population shows a much larger incidence ($\sim 20\%$) of early-type galaxies. This is the result of the IR selection, favouring the detection of galaxies with old stellar populations. Deeper SWIRE observations might reveal later type IR counterparts of the ACS sources, however this is not evident from the actual distribution of morphologies of the IRAC sources with the I-band magnitude: the percentage of early-type objects in bins of magnitude in the interval $[19.0, 25.0]$ takes values between 15% to 45% but without demonstrating any specific trend.

4.2 Model number counts

We now compare the statistical observables derived from our Spitzer IRAC dataset with simple evolutionary models. While the details on the models are more extensively described in Rodighiero et al. (2005, in prep.), we provide here a summary of our general approach. We adopt in the following H_0=70, Ω_M=0.3, $\Omega_\Lambda = 0.7$.

In our approach four main galaxy classes are considered: spheroids, quiescent spirals, an evolving population of irregular/merger systems (hereafter starburst population), and minor contributions from AGN.

The SED templates describing the spectral shapes at different galactic ages, needed to calculate the K-corrections, have been computed using the stellar population synthesis code GRASIL (Silva et al. 1998). We adopt a Salpeter IMF with a lower limit $M_l = 0.15 M_\odot$ and a Schmidt-type law for the star formation (SF) rate: $\Psi(t) = \nu M_g(t)$, where ν is the efficiency and $M_g(t)$ is the residual mass of gas. A further relevant parameter is the timescale t_{infall} for the infall of primordial gas. The evolution patterns for the models considered here are obtained with the following choices of the parameters. For early-types: $t_{infall} = 1\ Gyr$, $\nu = 1.3\ Gyr^{-1}$; for late-types: $t_{infall} = 4\ Gyr$, $\nu = 0.6\ Gyr^{-1}$. The corresponding SF law for ellipticals have a maximum at galactic ages of 1.4 Gyr, and is truncated at 3 Gyr to mimic the onset of a galactic wind. For late-type galaxies, the peak of the SF occurs at 3 Gyr. The parameters assumed to reproduce the spectra of spirals and irregular galaxies are that of a typical Sb spiral. This may not be very representative of an evolving population during a starburst phase, however, given the spectral region considered in this work, our assumption is still a good approximation. We have then generated two grids of model SEDs for both early- and late-types, spanning a range of ages from 0.1 to 15 Gyr.

For the local luminosity function we have made use of that estimated by Kochanek et al. 2001 for both early-type and late-type galaxy classes and derived from a K-band selected sample taken from the Two Micron All Sky Survey (2MASS), including 4192 low-redshift ($z \sim 0.02$) galaxies.

Our schematic model for both the spheroidal and the spiral population assumes that the galaxy comoving number density keeps constant once the population is formed at a given redshift, while the galaxy luminosities evolve following their evolutionary stellar content.

On the other hand, the analysis of deep galaxy surveys in the K-band (Cassata et al. 2005; Franceschini et al. 2005 in prep.) indicates the presence of a numerous population of irregular/merging systems at high-redshifts, likely requiring luminosity as well as density evolution going back in cosmic time. We then add a population of starbursts whose density $\rho(z)$ evolves with the following rule:

$$\rho(z) \propto \rho(z_0) \times (1+z) \tag{4}$$

for $z < 1$, and constant above, and whose luminosities $L(z)$ increases as

$$L(z) \propto L(z_0) \times (1+z)^{1.3} \tag{5}$$

for $z < 2$, and constant above.

Before detailing the comparison of our model predictions with the observed statistics derived from our sample, we need to consider how a morphological selection correlates with a classification based on the intrinsic SED of galaxies. A convenient way to directly check this point is to look at the colours of the SEDs templates assumed by the model, in order to verify if they are representative of the morphologically selected spheroids and spiral populations.

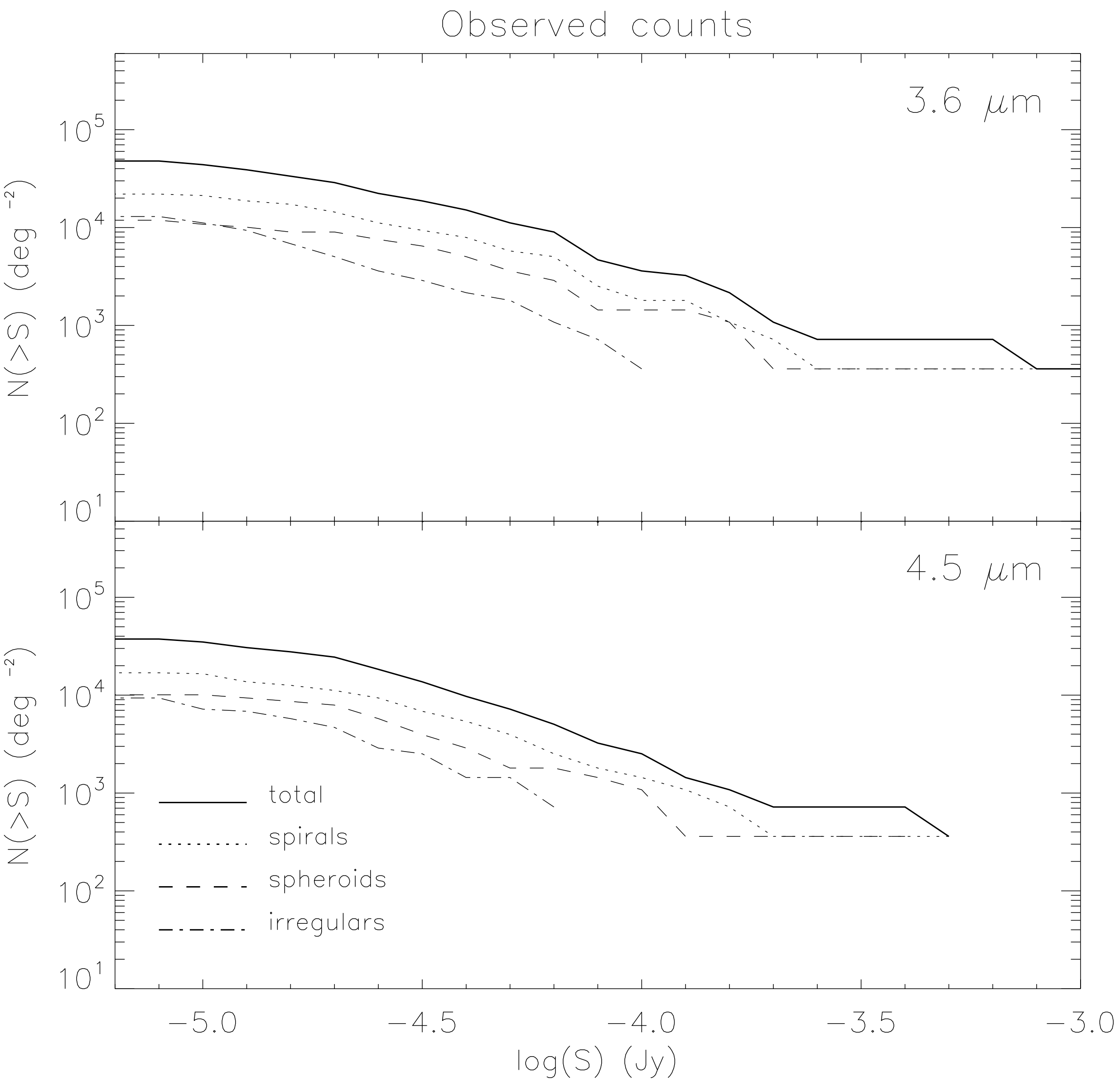

Figure 9. Observed cumulative 3.6 (upper panel) and 4.5 µm (lower panel) counts for the various types of objects (as classified by visual inspection) and their total number (solid line).

As an example, in Fig. 11 we report the I-4.5 µm versus the g- 3.6 µm observed colour-colour plot, compared with the model templates.

The blue dots mark the visually classified late-type sources; red open circles are spheroids; green triangles are galaxy pairs. The curves show the evolutionary tracks corresponding to an elliptical and spiral SED at different ages (red solid - dotted - dashed lines: ellipticals of 2, 5 and 13 Gyr, respectively; blue solid - dashed - dotted: Sa, Sb and Sc, respectively). Fig. 11 suggests that morphologically selected elliptical galaxies preferentially populate the reddest region of the observed colour distribution. However, the colour degeneracy between age and extinction prevent us to have an unambiguous photometric selection for spheroids. As shown in the figure, contamination from later type extincted sources is unavoidable. Similarly, those spheroids that have undergone recent episodes of star formation have bluer colours and then fall within the region preferentially populated by late-types.

This analysis suggests that a pure morphological selection is not obviously comparable with a colour criterion, and that a given amount of contamination affects such kind of comparison. However, assuming that the template SEDs discussed above are reasonably representative of the morphological classes, we have investigated the statistical properties of the SWIRE sample and compared them with the predic-

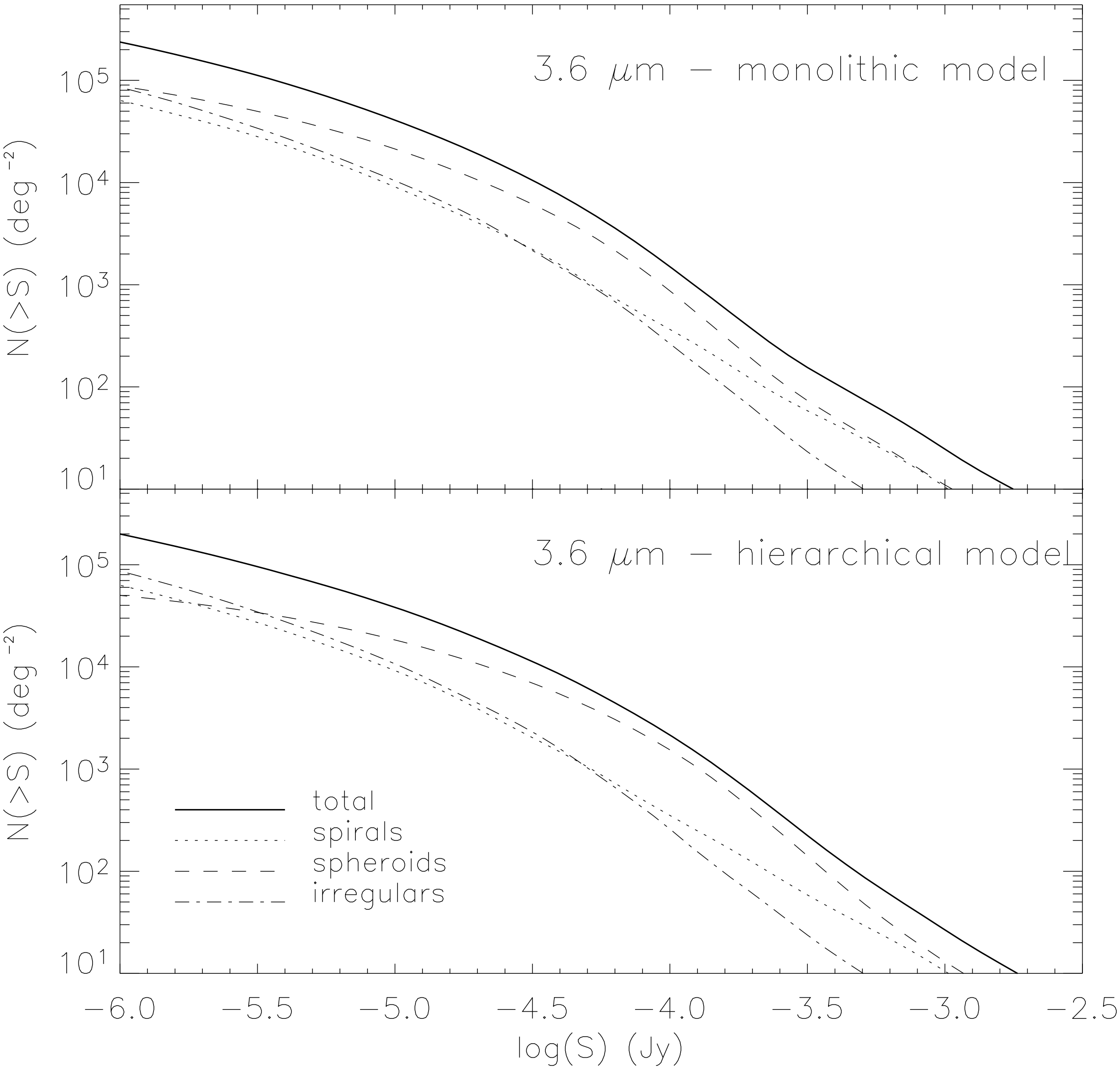

Figure 10. Cumulative model counts at 3.6 μm for the *monolithic* (upper panel) and *hierarchical* (lower panel) models. The counts are reported here for the various different morphological classes as indicated in the line caption. Note that *monolithic* and *hierarchical* scenaria only differ in the spheroids' (and therefore also total) counts.

tions of our modelistic approach. Any conclusion based on this analysis has to be taken with caution, in particular for the specific properties of the different spheroidal and spiral/irregular classes.

We now explore two schemes for the formation of spheroidal galaxies. The first one corresponds to the classic – *monolithic* – scenario assuming a single impulsive episode for the formation/assembly of the field ellipticals, occurring at a high redshift ($z_{form} > 2.5$, e.g. Daddi et al. 2000 and Cimatti et al. 2002). In our current implementation, we assume a redshift of formation $z_{form} = 3.0$.

The second model for spheroidal galaxies – the *hierarchical* model – describes a situation in which massive ellipticals form (or at least assemble) at lower redshifts through the merging of smaller units down to recent epochs. In such a case the formation of early-type galaxies is spread in cosmic time. Very schematically, we achieve this by splitting the local spheroidal galaxies into several sub-populations, each one forming at different redshifts. All sub-populations have the same mass function but different normalizations, whose total at $z = 0$ has to reproduce the local luminosity function. This model is being tested against deep galaxy surveys in the K band (K20 Cimatti et al. 2002, HDFS Franceschini et al. 1998 and Rodighiero et al. 2001;

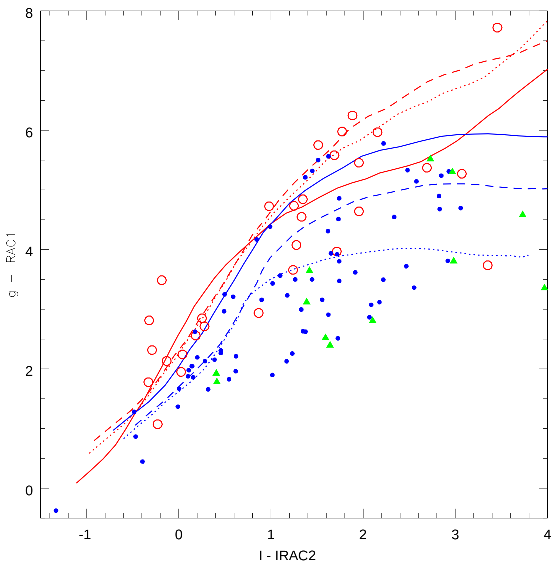

Figure 11. Colour-colour diagram (g-IRAC1) vs (I-IRAC2) showing the location of the spheroids, spirals and pairs (in open circles, dots and filled triangles, respectively) and the model evolutionary tracks of ellipticals and spirals (in red and blue lines, respectively; for details about the line coding, see text).

GDDS Abraham et al. 2004). In our current implementation, the bulk ($\sim$ 60%) of the early-type mass function is assembled in the redshift interval $1.1 < z < 1.6$, with additional fractions being formed at higher and lower z. At this stage, for simplicity, we do not consider extinction effects during the star formation phase. We defer to Franceschini et al. (2005) and Rodighiero et al. (2005) for a more detailed discussion and additional applications of this modeling.

Fig. 10 shows the predicted cumulative number counts at 3.6 µm for the hierarchical and monolithic scenario, respectively. The difference is essentially in the spheroidal population. The main value of these models is to provide, particularly for the spheroidal and normal spiral components, the simplest possible extrapolations of the local luminosity functions back in cosmic time. The addition of a strongly evolving population of irregular/mergers is instead motivated by the need to reproduce, at least at the zero-th order, the observed statistics from deep K-band counts (Franceschini et al. 2005). In any case, these simple models predict that spheroidal galaxies would make important contributions to the Spitzer/IRAC counts.

4.3 Discussion

We report in Figs. 12 and 13 detailed comparisons, with model expectations, of the SWIRE observed integral counts at 3.6 and 4.5 µm for the various morphological classes in the *Tadpole* ACS image. Only a general distinction between spheroidal and non-spheroidal systems is made here, the latter including both spirals and irregulars/mergers. The observed counts are shown down to 10 µJy, roughly the 90% completeness limits of SWIRE IRAC1 band. The solid and dashed lines correspond to the hierarchical and monolithic scenario, respectively, while the dotted lines show the observed number counts. More precisely, the two dotted lines appearing in these figures for each morphological class correspond to the lower and upper boundaries on the source real density which have been discussed in Sect. 3.2. The upper and lower limits in this case of spheroids correspond to the CAS analysis and visual inspection, respectively, whereas in the case of the remaining classes (marked in the plot as "other") the upper limit is due to visual inspection and the lower to the CAS parameters. The observed IRAC1 counts given by Fazio et al. (2004) are shown for comparison (marked as diamonds in Figs. 12 and 13). Note that, given the modest statistics of our source sample, the detailed shapes of the counts (showing bumps and humps at the bright end of the counts) are not to be considered as significant.

Despite the very small size of our sample, the total counts are in good agreement with those observed by Fazio et al. (2004) over a much larger area (several square degrees), especially the 3.6 µm counts. In the case of the 4.5 µm counts, the statistics start being really poor as we are dealing with only 130 objects detected in this band. The observed spheroidal counts are in very good agreement with those predicted by the hierarchical scenario while the monolithic model clearly predicts more early-type objects and steeper counts. However, while the models predict counts essentially dominated by ellipticals (see Fig. 10), we find a striking excess of late-type galaxies and merger-irregulars to dominate particularly at the faintest fluxes where the counts of spheroidal galaxies appear to converge rapidly.

The observed spheroids counts are inconsistent with the monolithic predictions that implies too steep number counts and would exceed the observed counts at the faint fluxes. A coeval origin for spheroids at reasonable redshift, therefore, seems to produce excess counts compared to observations. Changing the stellar IMF during the star-formation phase from a Salpeter to e.g. a Scalo (1986) distribution would probably somehow easy the inconsistency (Cimatti et al. 2002), but at the cost of not explaining by large factors the extragalactic background radiation intensities (Madau & Pozzetti 2000, Franceschini et al. 2001) and the observed metalicities of intracluster plasmas (Muskotzky & Loewenstein 1997).

The slight observed deficit of spheroids with respect to the hierarchical predictions, more noticeable in the case of the 4.5 µm counts, could suggest that the simple assumption of a protraction of the formation phase of ellipticals and of their progressive disappearance already starting at z=1 may not be entirely sufficient to bring the statistics into agreement. An additional factor to consider is likely the dust extinction effects during the main phases of star formation.

On the other hand, the observed numbers of spiral and irregular galaxies are larger than that predicted by our simple evolutionary scheme. This simple model, roughly fitting the K-band galaxy statistics, falls short of the observed counts at both 3.6 and 4.5 µm. Part of this inconsistency may be due to our lack of consideration of dust and PAH (e.g. the 3.3 µm feature) emission components.

Very qualitatively, it might be tempting to interpret the observed excess population of irregulars and mergers and their inferred strong cosmological evolution as the progenitors of spheroidal galaxies, the rapid relaxation and gas exhaustion following the merger bringing to a sudden ap-

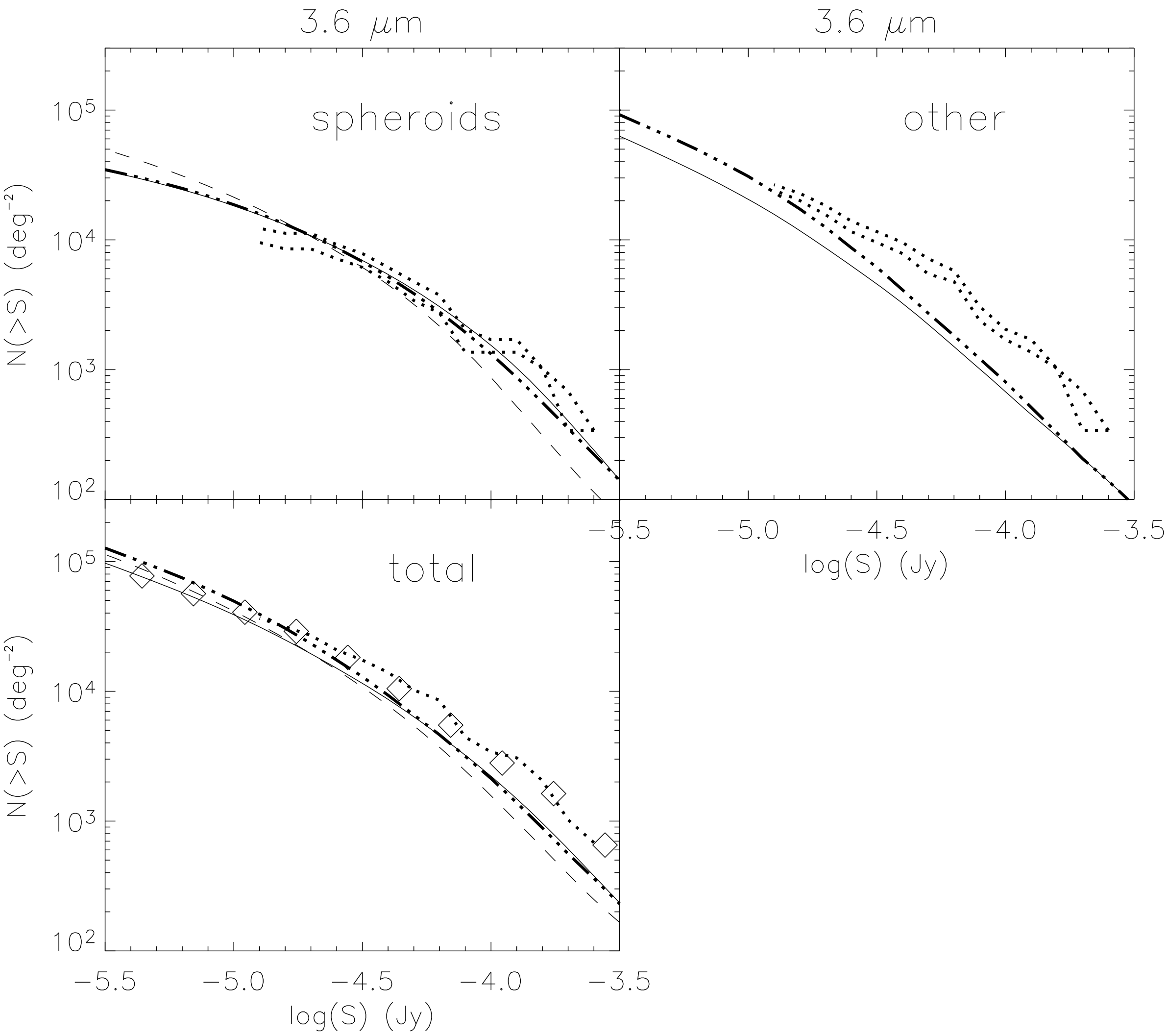

Figure 12. Comparison of the observed (dotted line) and model (solid and long-dashed lines for the hierarchical and monolithic scenario, respectively) 3.6 µm number counts. The upper and lower limits for the observed counts are given by the CAS parameter analysis and visual inspection, respectively, as discussed in the text. Note that, compared with Fig. 10, the spiral and irregular galaxies are here combined in the "other" class. The diamonds in the lower panel represent the IRAC1 counts given by Fazio et al. (2004). The dashed-triple-dot line shows the predictions of an improved version of the model presented in Xu et al. 2003 (see text for details).

pearance of a spheroid. Obviously, any more quantitative conclusion will require much further information on source identifications and redshifts.

Because of the inconsistency between observed and model late-type galaxies, we further compared our results with an improved version of the model presented by Xu et al. (2003). In its original version this model over-predicted the 24 µm counts (for a detailed discussion see Shupe et al. 2005). In order to correct for this effect but still fit the 15 µm *ISO* counts the evolution rate of starburst galaxies was lowered with respect to the old model and the strength of the PAH features in the wavelength range of 5 µm $< \lambda <$ 12 µm was raised by a factor of 2 in the SEDs of both starburst and normal galaxies. Thus, the predicted late-type counts are still below the observed limits but are higher by a factor of ~ 1.5 than those predicted by our simple hierarchical scenario. They are shown in dashed-triple-dot line in Figs. 12 and 13. This reinforces our previous statement about the deficit of model late-type galaxies reflecting the lack of PAH emission from the models presented in Section 4.2.

5 CONCLUSIONS

This work presents results of a morphological analysis of a small subset of the Spitzer Wide-area InfraRed Extragalactic survey (SWIRE) galaxy population. Our sample is flux-limited at 3.6 and 4.5 µm and consists of 156 galaxies with IRAC1 and IRAC2 fluxes larger than 10 µJy. Our analysis is based on public ACS data taken inside the SWIRE N1 field. We distinguish two very general classes of galaxies, bulge- and disk- dominated ones, the first class being referred at

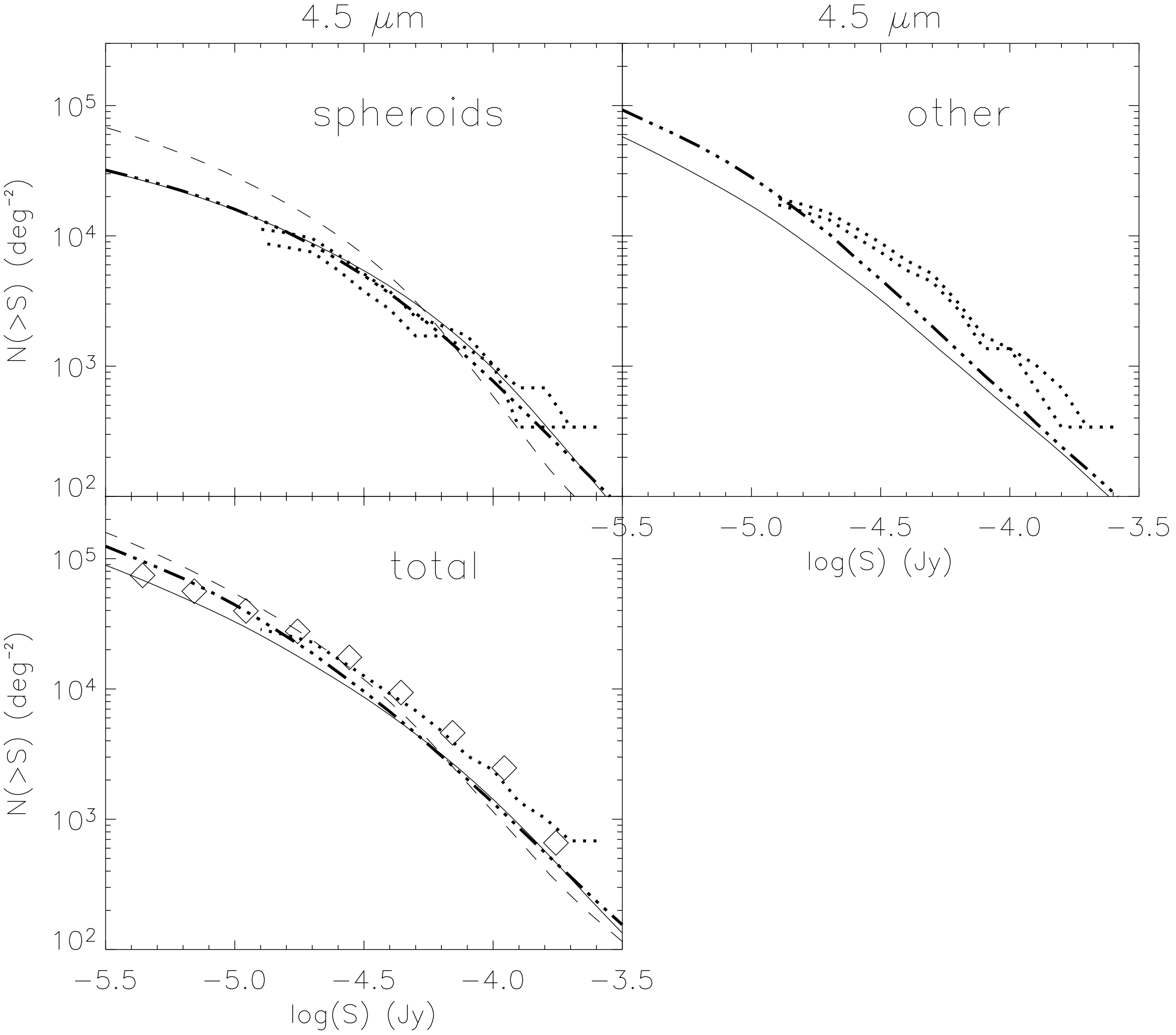

Figure 13. Same as Fig. 12 but for 4.5 μm.

with the general term "spheroids" and the second one containing everything from spirals to irregulars and pairs. The existence of a large fraction of disk galaxies and interacting systems in the sample under study ($\sim 80\%$) already suggests that elliptical galaxies assemble late by merging processes.

The *monolithic* and *hierarchical* models checked against this data set considerably under-predict the number of late-type galaxies. The observed 3.6 μm early-type counts are in very good agreement with the estimations of the hierarchical scenario, while the 4.5 μm early-type counts marginally agree with the predictions of the same model (they lie slightly below the model predictions). This does not come as a surprise as we are working with a sample selected at wavebands where we would expect their most efficient detection. The monolithic predictions imply much steeper counts and fail almost totally in reproducing the observations.

Additional comparison of the dataset with another model available in the literature (Xu et al. 2003) suggested that dealing in an appropriate way with some of the models deficiencies like the dust or PAH emission components should result in a better agreement. It should be mentioned that the model predictions may depend significantly on the assumed stellar IMF (see e.g. Cimatti et al. 2002), although the one we adopted here should be rather representative of the main phases of star formation. The model itself is rough and the predicted counts should not be taken at face value but rather be considered indicative of the expected tendencies.

This ACS data set is the deepest available, as of today, in any of the SWIRE fields and therefore the results of the present analysis are of great importance for the understanding of the SWIRE galaxy population. Due to the small size of our sample, however, we cannot be very conclusive and can only outline some general tendencies. We would like to point out a number of potential sources of uncertainty in the interpretation of our results, namely: i) the way that large-scale structure may influence the results, given the particularly small size of the ACS field; ii) the possible existence of heavily obscured, by dust, ellipticals at the stage of their formation; iii) the assumption of *a priori* values instead of a χ^2 minimization on some of the model parameters; iv) the uncertainties on the exact shape of the SEDs of the various galaxy types in these newly explored, IR wavelengths; and finally v) the requirement of hybrid models of the two extreme schemes (monolithic and hierarchical) considered here in order to better reproduce the observed counts.

ACKNOWLEDGMENTS

This work is based on observations made with the *Spitzer Space Telescope*, which is operated by the Jet Propulsion Laboratory, California Institute of Technology under NASA contract 1407. Support for this work, part of the Spitzer Space Telescope Legacy Science Program, was provided by NASA through an award issued by the Jet Propulsion Laboratory, California Institute of Technology under NASA contract 1407.

ACS was developed under NASA contract NAS 5-32865, and this research has been supported by NASA grant NAG5-7697. We are grateful for an equipment grant from Sun Microsystems, Inc. The Space Telescope Science Institute is operated by AURA Inc., under NASA contract NAS5-26555.

This work was supported in part by the Spanish Ministerio de Ciencia y Tecnologia (Grants Nr. PB1998-0409-C02-01 and ESP2002-03716) and by the EC network "POE" (Grant Nr. HPRN-CT-2000-00138).

We would like to thank N. Benitez for making publicly available the reduced ACS image used in this work.

Finally we thank the anonymous referee for the precise and detailed report that greatly improved the presentation of our work.

REFERENCES

Abraham R.G. et al. 1996, MNRAS, 279, 47
Abraham R.G. et al., 2004, AJ, 127, 2455
Benitez N. et al., 2004, ApJ, 150, 1
Bertin E., Arnouts S., 1996, A&AS, 117, 393
Cassata P. et al., 2005, MNRAS, 357, 903
Chiosi C., Carraro G., 2002, MNRAS, 335, 335
Cimatti A. et al., 2002, A&A, 391 1
Cimatti A. et al., 2004, Nature, 430, 184
Cole A., Lacey C.G., Baugh C.M., Frenk C.S., 2000, MNRAS, 319, 204
Conselice C.J., Bershady M.A., Jangren A., 2000, ApJ, 529, 886
Conselice C.J., 2003, ApJS, 147, 1
Conselice C.J., Bershady M.A., Dickinson M., Papovich C., 2003, AJ, 126, 1183
Daddi E., Cimatti A., Renzini A., 2000, A&A, 362, L45
Dickinson M., Papovich, C., Ferguson, H.C., Budavari, T., 2003 ApJ, 587, 25
Eggen O. J., Lynden-Bell D., Sandage A. R., 1962, ApJ, 136, 748
Fazio G.G. et al., ApJS, 154, 39
Ford H.C. et al., 1998, SPIE, 3356, 234
Franceschini A. et al., 1998, ApJ, 506, 600
Franceschini A. et al., 2001, A&A, 378, 1
Kauffmann G., Charlot S., White S.D.M., 1996, MNRAS, 283, 117
Kauffmann G., Charlot S., 1998, MNRAS, 297, L23
Kochanek C.S. et al., 2001, ApJ, 560, 566
Larson R., 1975, MNRAS, 173, 671
Longhetti M., Bressan A., Chiosi C., Rampazzo R., 2000, A&AS, 353, 917
Lonsdale C. et al., 2004, ApJS, 154, L54
Lotz J. Primack J., Madau P., 2004, AJ, 128, 163
Madau P., Pozzetti L., 2000, MNRAS, 312, 9
Mushotzky R.F. & Loewenstein M. 1997, ApJ, 481, L63
Papovich C. et al., 2003, ApJ, 598, 827
Peng C.Y., Ho L.C., Impey C.D., Rix H.-W., 2002, ApJ, 124, 266
Pignatelli E., Fasano G., Cassata P., 2005, A&A, submitted
Rodighiero G., Franceschini A., Fasano G., 2001, MNRAS, 324, 491
Rowan-Robinson M., 2001, ApJ, 549, 745
Rowan-Robinson M. et al., 2005, AJ, 129, 1183
Scalo J.M., 1986, Fundamentals of Cosmic Physics, 11, 1
Sérsic J., 1968, *Atlas de Galaxias Australes Cordoba: Observatorio Astronomico*
Shupe D.L. et al., AJ, submitted
Silva L., Granato G.L., Bressan A., Danese, L., ApJ, 509, 103
Somerville R.S., Primack J.R. 1999, MNRAS, 310, 1087
Somerville R.S. et al., 2004, ApJ, 600, L135
Surace J.A. et al., 2005, in prep.
Thomas D., Maraston C., Bender R. Mendes de Oliveira C., ApJ, 2005, 621, 673
Windhorst R. A. et al., 2002, ApJS, 143, 113
Wirth G.D. et al., 2004, AJ, 127, 3121
White S.D.M., Rees M.J. 1978, MNRAS , 183, 341
White S.D.M., Frenk C.S., 1991, ApJ, 379, 52
Xu C.K. et al., 2003, ApJ, 587, 90